



## RESEARCH LETTER

10.1029/2018GL078814

### Key Points:

- The India-Eurasia collision zone would suffer from about 11  $M_w \geq 7.5$ , 36  $M_w \geq 7.0$ , 109  $M_w \geq 6.5$ , and 326  $M_w \geq 6.0$  shallow earthquakes per 100 years
- Shallow seismicity forecast provides a promising approach to help distinguish between block and continuum models for crustal deformation
- The west-central Himalaya and the central Altyn Tagh fault are undergoing high earthquake risk

### Supporting Information:

- Supporting Information S1
- Data Set S1
- Data Set S2
- Data Set S3
- Data Set S4
- Data Set S5
- Data Set S6
- Data Set S7
- Data Set S8
- Data Set S9
- Data Set S10
- Data Set S11
- Data Set S12
- Data Set S13
- Data Set S14
- Data Set S15
- Data Set S16
- Data Set S17
- Data Set S18
- Data Set S19
- Data Set S20

### Correspondence to:

Y. Lou and J. Geng,  
ydlou@whu.edu.cn;  
jgeng@whu.edu.cn

### Citation:

Zheng, G., Lou, Y., Wang, H., Geng, J., & Shi, C. (2018). Shallow seismicity forecast for the India-Eurasia collision zone based on geodetic strain rates. *Geophysical Research Letters*, 45. <https://doi.org/10.1029/2018GL078814>

Received 19 MAY 2018

Accepted 10 AUG 2018

Accepted article online 20 AUG 2018

## Shallow Seismicity Forecast for the India-Eurasia Collision Zone Based on Geodetic Strain Rates

Gang Zheng<sup>1,2</sup> , Yidong Lou<sup>1,2</sup> , Hua Wang<sup>2,3</sup> , Jianghui Geng<sup>1,2</sup> , and Chuang Shi<sup>4</sup>

<sup>1</sup>GNSS Research Center, Wuhan University, Wuhan, China, <sup>2</sup>Collaborative Innovation Center of Geospatial Technology, Wuhan University, Wuhan, China, <sup>3</sup>Department of Surveying Engineering, Guangdong University of Technology, Guangzhou, China, <sup>4</sup>School of Electronic and Information Engineering, Beihang University, Beijing, China

**Abstract** Geodetic strain rates from increasing Global Positioning System data provide a promising approach for seismicity forecast. With the strain rate field presented in Zheng et al. (2017, <https://doi.org/10.1002/2017JB014465>) derived from the most complete and up-to-date Global Positioning System data set in the India-Eurasia collision zone, we forecast the shallow seismicity of this region, and infer that about 11  $M_w \geq 7.5$ , 36  $M_w \geq 7.0$ , 109  $M_w \geq 6.5$ , and 326  $M_w \geq 6.0$  earthquakes may occur here every 100 years. We indicate that shallow seismicity forecast may be able to help us distinguish between block and continuum models, and block model cannot well describe the kinematics of the Tibetan Plateau, Tien Shan, West Mongolia, North China, and Myanmar. We suggest that the regions with high forecasted earthquake rates but lack of historical earthquakes are undergoing high seismic risk, such as the west-central Himalaya (overdue for  $M_w \geq 7.5$  earthquakes, possibly  $M_w \geq 8.0$ ) and the central Altyn Tagh fault (overdue for  $M_w \geq 7.0$  and  $M_w \geq 7.5$  earthquakes).

**Plain Language Summary** Seismicity has brought enormous losses of life and property to human, especially to the India-Eurasia collision zone. The society is eager for a good seismicity forecast to help reduce the losses from earthquakes. Geodetic strain rates from increasing Global Positioning System data provide a promising approach for the seismicity forecast. In this study, we forecast the shallow seismicity of the India-Eurasia collision zone in different magnitude ranges based on the most complete and up-to-date Global Positioning System data set for this region. The forecast results show that the India-Eurasia collision zone may suffer from about 11  $M_w \geq 7.5$ , 36  $M_w \geq 7.0$ , 109  $M_w \geq 6.5$ , and 326  $M_w \geq 6.0$  shallow earthquakes every 100 years. We associate shallow seismicity forecast with the long-term debate between block and continuum models for the crustal deformation in the India-Eurasia collision zone, and suggest that the forecast results may help clarify the debate. Also, we indicate that the combination of the forecast results and the historical seismic catalog can be used to identify seismic gaps, such as the west-central Himalaya that is overdue for  $M_w \geq 7.5$  earthquakes (possibly  $M_w \geq 8.0$ ) and the central Altyn Tagh fault that is overdue for  $M_w \geq 7.0$  and  $M_w \geq 7.5$  earthquakes.

## 1. Introduction

The India-Eurasia collision zone is one of the most active tectonic regions in the world with numerous faults and widespread large earthquakes (Molnar & Tapponnier, 1975; Tapponnier & Molnar, 1977). After the 2010  $M_w7.0$  Haiti earthquake (Bilham, 2010), TIME published an article to review the top 10 deadliest earthquakes in human history (<http://content.time.com/time/specials/packages/completelist/0,29569,1953425,00.html>). To our surprise, half of the 10 earthquakes happened in the India-Eurasia collision zone: The 1556  $M8.0$  Huaxian earthquake, the deadliest earthquake ever recorded by human, killed about 830,000 people; the 1920  $M_w7.8$  Haiyuan earthquake caused over 200,000 deaths; the 1976  $M_w7.8$  Tangshan earthquake brought over 10-billion-renminbi economic losses and killed about 240,000 people; the 2005  $M_w7.6$  Kashmir earthquake led to about 79,000 deaths; and the 2008  $M_w7.9$  Wenchuan earthquake killed more than 87,000 people and resulted in about 86-billion-dollar economic losses. Seismicity has brought enormous losses of life and property to human, especially to the India-Eurasia collision zone. Thus, the society is eager for a good seismicity forecast to help reduce the losses from earthquakes.

A straightforward forecast method is extrapolating the past earthquake catalog with appropriate smoothing algorithms (e.g., Kagan & Jackson, 1994, 2000, 2011; Wang et al., 2011). Yet this method may locally fail to record the representative level of the seismicity due to the short or incomplete historical seismic catalog.

Therefore, some forecast studies focused on active faults (e.g., Field et al., 2013; Petersen et al., 2014). However, such fault-based models cannot work well in many countries and regions owing to the incomplete fault maps. Otherwise, damaging earthquakes occur continuously in unexpected locations (England & Jackson, 2011), even in the stable continental regions (Calais et al., 2016; Johnston et al., 1994), such as the 1755 Lisbon, the 1811–1812 New Madrid, and the 1886 Charleston earthquakes (Johnston, 1996).

With the improvement of geodetic measurements such as Global Positioning System (GPS) observations, it is promising to forecast the seismicity from geodetic strain rate fields. The strain rates can be converted to seismic moment rates, which can further be used to forecast the future seismicity (e.g., Bird & Kreemer, 2015; Bird et al., 2010). The main advantage of this forecast approach is that the strain rate field mainly depends on the spatial resolution of geodetic measurements, so that it can overcome the problems of past methods limited by incomplete catalogs of historical earthquakes and tectonic fault maps. Based on the Global Strain Rate Map (GSRM) from Kreemer et al. (2003), Bird et al. (2010) forecasted the global shallow seismicity under the Seismic Hazard Inferred From Tectonics (SHIFT) hypotheses (Bird & Liu, 2007), in which *shallow* referred to all hypocentroids located no more than 70 km below sea level; Bird and Kreemer (2015) revised this forecast using the upgraded version of the GSRM derived from far more GPS data and improved models by Kreemer et al. (2014); Bird et al. (2015) combined the revised forecast with a smoothed-seismicity forecast computed by the methods of Kagan and Jackson (1994, 2000, 2011) to obtain a hybrid forecast. However, these studies were aimed at global shallow seismicity, which did not have detailed analyses for the India-Eurasia collision zone.

Recently, Zheng et al. (2017) presented the most complete and up-to-date GPS data set in the India-Eurasia collision zone, and calculated the strain distribution of this region. Using the GPS-derived strain rate field given by Zheng et al. (2017), we apply the method in Bird and Kreemer (2015) to forecast the shallow seismicity in the India-Eurasia collision zone. Then we evaluate the quality of our forecast results. Subsequently, we apply the forecast results to the issue of block versus continuum models, and discuss two seismic gaps—the west-central Himalaya and the central Altyn Tagh fault, which have high forecasted earthquake rates but are lack of historical earthquakes.

## 2. Method and Results

We apply the SHIFT\_GSRM2f model preferred by Bird and Kreemer (2015) to make our regional shallow seismicity forecast in the India-Eurasia collision zone. The main steps of the forecast are outlined as follows: First, resample the principal strain rate field presented by Zheng et al. (2017; as shown in their Figure 4) into a rectangular mesh with  $0.2^\circ \times 0.25^\circ$  (latitude  $\times$  longitude) cell; second, calculate the seismic moment rate of each rectangular cell using the principal strain rates based on the coupled seismogenic thickness (the product of seismogenic thickness and dimensionless seismic coupling coefficient) of the most comparable class of plate boundary; third, convert the seismic moment rate to a raw shallow earthquake rate based on the frequency-magnitude distribution of the most comparable class of plate boundary; fourth, refine the empirical constants for the forecast, by comparing the sum of the raw forecasted shallow earthquake rates of all the cells in each kind of the tectonic zones with the actual shallow earthquake rate of the 1977–2016 Global Centroid Moment Tensor (GCMT) catalog in the corresponding tectonic zone (the classification of the tectonic zones is from Kagan et al., 2010); finally, calibrate the forecast with the refined empirical constants to obtain the final forecasted shallow earthquake rates. For more details of the steps, please refer to Bird and Kreemer (2015).

The time span of the GCMT catalog used in Bird and Kreemer (2015) was 1977–2013, while we use the 1977–2016 GCMT catalog; Bird and Kreemer (2015) was based on the GSRM from Kreemer et al. (2014), while we use an updated geodetic strain rate field for the India-Eurasia collision zone presented by Zheng et al. (2017). Except for the seismic catalog and the strain rate field, we keep consistent with Bird and Kreemer (2015) in other aspects. That is to say, we adopt the built-in values in the SHIFT\_GSRM2f model for the critical coupled seismogenic thicknesses and corner magnitudes, which were taken from Table 5 of Bird and Kagan (2004). This table has columns for each of the seven plate-boundary classes defined in the PB2002 model of Bird (2003). The India-Eurasia collision zone involves three of the seven classes, that is, continental convergent boundary, continental transform fault, and continental rift boundary. The coupled seismogenic thickness values for continental convergent boundary, continental transform fault, and continental rift boundary

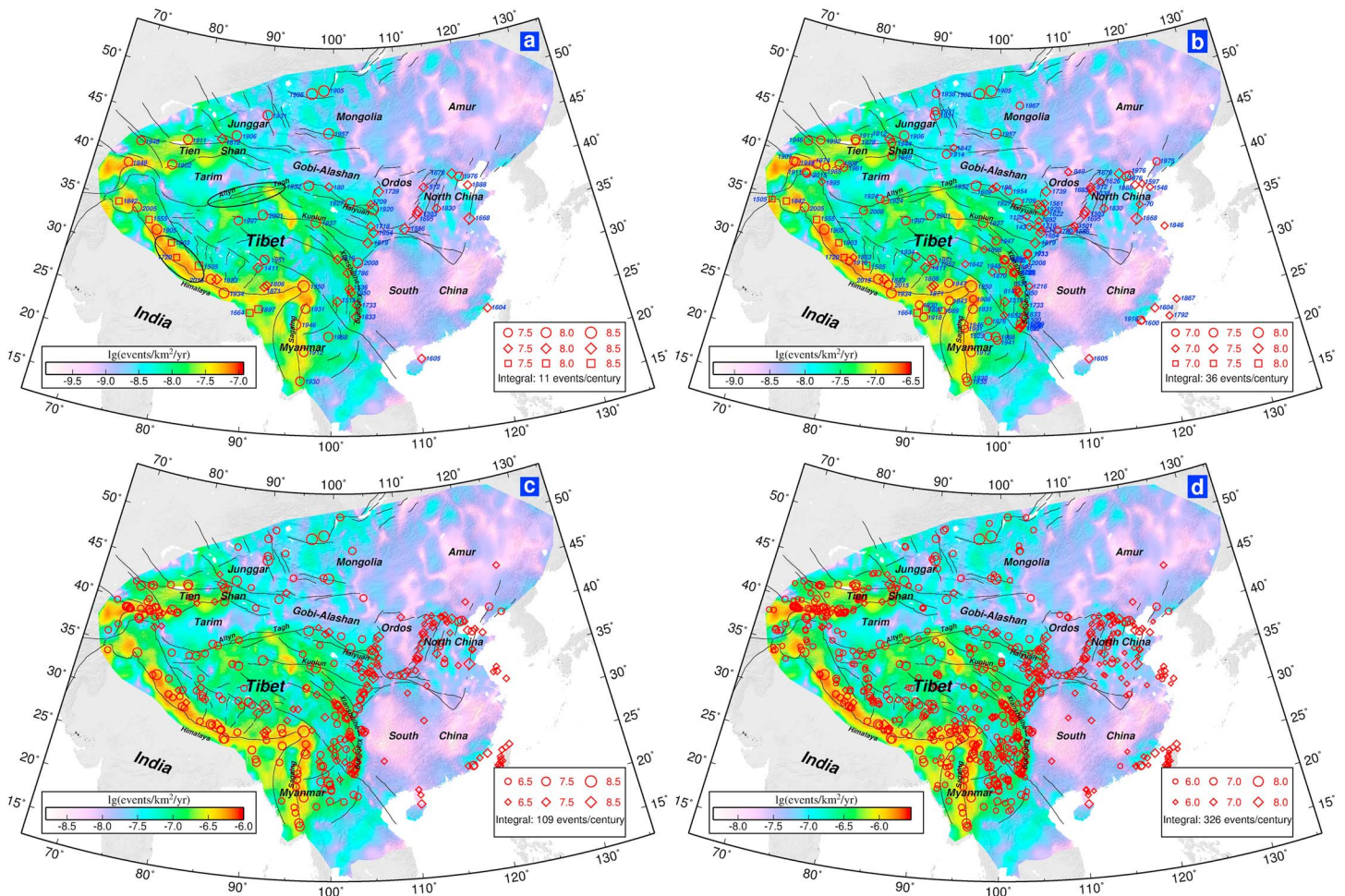


**Figure 1.** The forecast result of the shallow seismicity in the India-Eurasia collision zone. (a)–(d) are for  $M_w \geq 7.5$ ,  $M_w \geq 7.0$ ,  $M_w \geq 6.5$ , and  $M_w \geq 6.0$  shallow earthquakes, respectively. The red circles represent the earthquakes during 1900–2016 from the U.S. Geological Survey seismic catalog, and the red diamonds are the historical earthquakes in China continent during 2300 B.C. to 1900 recorded by China Earthquake Administration (Division of Earthquake Monitoring and Prediction, 1995). In (a) and (b), the red squares represent the earthquakes during 1500–1900 along the Himalaya except for those in China continent (Ambraseys & Douglas, 2004), and the blue numbers indicate the years of the earthquakes. The black ellipses in (a) represent the two seismic gaps discussed in section 3.3.

tectonic settings are  $18^{+7}_{-11}$ ,  $8.6^{+11}_{-4}$ , and  $3.0^{+7.0}_{-1.4}$  km, respectively (the question mark indicates that the upper limit is not found), and the corner-magnitude values for them are  $8.46^{+0.21}_{-0.39}$ ,  $8.01^{+0.47}_{-0.21}$ , and  $7.64^{+0.76}_{-0.26}$ , respectively. Note that the start time of the forecast follows the threshold time of the seismic catalog used in the forecast; thus, our forecast results are for the seismicity from 2017 onwards.

We carry out 20 forecasts for the India-Eurasia collision zone, including  $M_w \geq 7.9$ ,  $M_w \geq 7.8$ ,  $M_w \geq 7.7$ ,  $M_w \geq 7.6$ ,  $M_w \geq 7.5$ ,  $M_w \geq 7.4$ ,  $M_w \geq 7.3$ ,  $M_w \geq 7.2$ ,  $M_w \geq 7.1$ ,  $M_w \geq 7.0$ ,  $M_w \geq 6.9$ ,  $M_w \geq 6.8$ ,  $M_w \geq 6.7$ ,  $M_w \geq 6.6$ ,  $M_w \geq 6.5$ ,  $M_w \geq 6.4$ ,  $M_w \geq 6.3$ ,  $M_w \geq 6.2$ ,  $M_w \geq 6.1$ , and  $M_w \geq 6.0$  shallow seismicity forecasts. We store each forecast result in a gridded digital file. These files are available in the supporting information section and uploaded separately. The description of the file format can be found in the caption for Data Set S1 in supporting information S1. Figures 1a–1d show the forecast results of  $M_w \geq 7.5$ ,  $M_w \geq 7.0$ ,  $M_w \geq 6.5$ , and  $M_w \geq 6.0$  shallow seismicities, respectively. The forecast values represent the number of earthquakes per square kilometer per year.

Figures 1a–1d have similar spatial distribution patterns. As a whole, except for those along a few active structures in North China and the southeast coast of China, the forecast values in the east of the India-Eurasia collision zone are smaller than those in the west. The highest forecast values mainly lie in the southern margin of the western Tien Shan, and the Himalaya and Sagaing faults. The secondary values are broadly distributed in the Tibetan Plateau and Tien Shan.

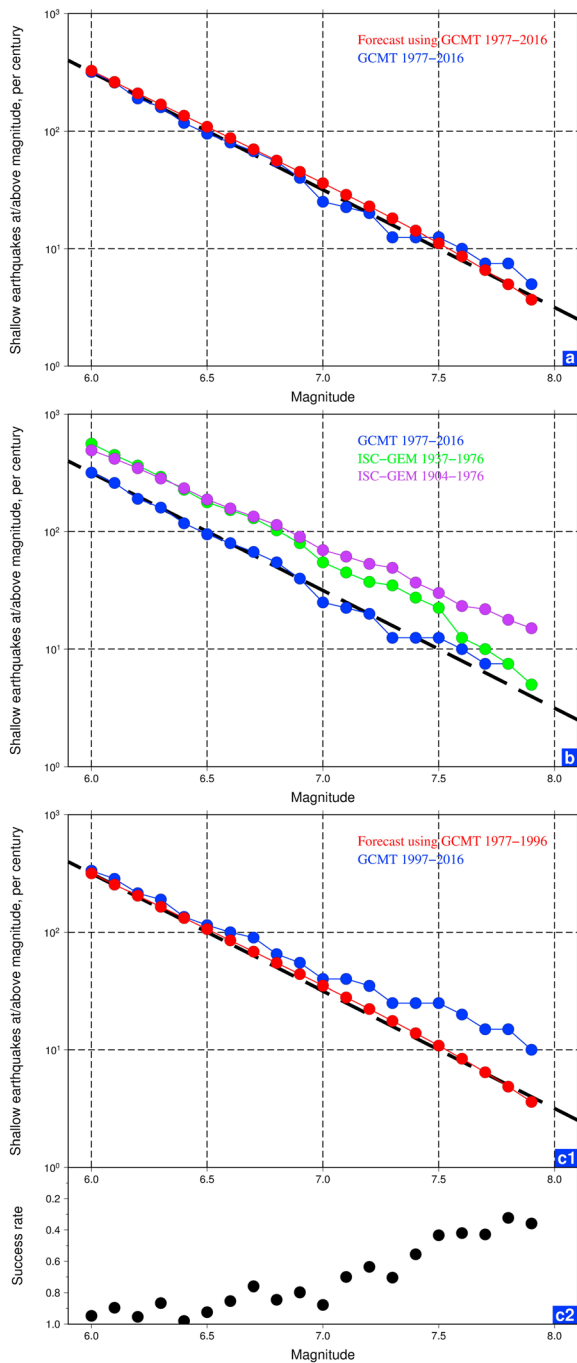


**Figure 2.** (a) The numbers of the shallow earthquakes every 100 years in different magnitude ranges forecasted with the 1977–2016 GCMT catalog (red circles) versus the actual situation shown by this catalog (blue circles). The reference line with a slope of  $-1$  is shown as a bold dashed line, the same in (b) and (c). (b) The numbers of the shallow earthquakes every 100 years in different magnitude ranges given by the 1977–2016 GCMT (blue circles), the 1937–1976 ISC-GEM (green circles), and the 1904–1976 ISC-GEM (purple circles) catalogs, respectively. (c) The numbers of the shallow earthquakes every 100 years in different magnitude ranges forecasted with the 1977–1996 GCMT catalog (red circles) versus the actual situation shown by the 1997–2016 GCMT catalog (blue circles), and the success rates of the forecast (black circles). GCMT = Global Centroid Moment Tensor; ISC-GEM = International Seismological Centre-Global Earthquake Model.

Integrating the 20 forecast results by area, we infer that the India-Eurasia collision zone would suffer from about 4  $M_w \geq 7.9$ , 5  $M_w \geq 7.8$ , 7  $M_w \geq 7.7$ , 9  $M_w \geq 7.6$ , 11  $M_w \geq 7.5$ , 14  $M_w \geq 7.4$ , 18  $M_w \geq 7.3$ , 23  $M_w \geq 7.2$ , 29  $M_w \geq 7.1$ , 36  $M_w \geq 7.0$ , 45  $M_w \geq 6.9$ , 56  $M_w \geq 6.8$ , 70  $M_w \geq 6.7$ , 88  $M_w \geq 6.6$ , 109  $M_w \geq 6.5$ , 136  $M_w \geq 6.4$ , 169  $M_w \geq 6.3$ , 210  $M_w \geq 6.2$ , 262  $M_w \geq 6.1$ , and 326  $M_w \geq 6.0$  shallow earthquakes every 100 years, shown as red circles in Figure 2a.

### 3. Discussion

#### 3.1. Assessment of the Quality of our Forecast Results

Figures 1a–1d all show that the forecast results using the 1977–2016 GCMT catalog are generally consistent with the distributions of the historical earthquakes recorded by other seismic catalogs, mainly including the 1900–2016 U.S. Geological Survey catalog and the catalog of the Chinese historical strong earthquakes during 2300 B.C. to 1900. However, this is only the qualitative consistency. In the following, we will assess the quality of our forecast results quantitatively.

First, we do a consistency check of the forecast results against the seismic catalog that is used for calibration in the forecast. We count the earthquakes in different magnitude ranges in the 1977–2016 GCMT catalog and then normalize the numbers to 100-year timescale, shown as blue circles in Figure 2a. We find that our forecast results based on this seismic catalog, shown as red circles in Figure 2a, are in good agreement with them.

Second, we would like to check our forecast results against other seismic catalog that is not used in the forecast process. In this case, we need to find a reliable seismic catalog except for the 1977–2016 GCMT catalog used in our forecast and then compare our forecast results with it. For the time before 1977, the International Seismological Centre-Global Earthquake Model (ISC-GEM) catalog may be the first option. We count the earthquakes in different magnitude ranges in the 1977–2016 GCMT and the 1937–1976 ISC-GEM catalogs (each catalog has a 40-year time span), and then normalize the numbers to 100-year timescale. The results are shown as blue and green circles in Figure 2b, respectively. The numbers of  $M_w \geq 7.9$ ,  $M_w \geq 7.8$ ,  $M_w \geq 7.7$ , and  $M_w \geq 7.6$  earthquakes every 100 years given by the two catalogs are generally similar, but for the magnitude ranges with a low threshold magnitude ( $M_w \leq 7.5$ ), a significant discrepancy exists between the results given by the two catalogs (Figure 2b). The ISC-GEM catalog we use is the newest version published in February 2018, which began to record earthquakes since 1904. Here we take the 1904–1936 ISC-GEM catalog into account as well, calculate the numbers of the earthquakes in different magnitude ranges in the 1904–1976 ISC-GEM catalog, and then normalize the numbers to 100-year timescale, shown as purple circles in Figure 2b. For all the magnitude ranges, the result derived from the 1904–1976 ISC-GEM catalog has an apparent bias relative to that shown by the 1977–2016 GCMT catalog (Figure 2b). We suggest that relatively large magnitude uncertainties in the 1904–1976 ISC-GEM catalog may affect the accuracy of the results, while those derived from the 1977–2016 GCMT catalog should be more reliable. But on the other hand, the time span of the GCMT catalog is short at present.

Given the above, in order to implement our plan, we divide the 1977–2016 GCMT catalog into two parts with the same time span—one from 1977 to

1996 and the other from 1997 to 2016. We then compare the forecast results based on the 1977–1996 GCMT catalog with the actual situation shown by the 1997–2016 GCMT catalog, and use  $R = 1 - |N_{\text{forecast}} - N_{\text{catalog}}| / N_{\text{catalog}}$  to calculate the success rates ( $R$ ) of the forecast results. Here  $N_{\text{forecast}}$  is the number of the earthquakes above and equal to the threshold magnitude every 100 years forecasted with the 1977–1996 GCMT catalog, shown as red circles in Figure 2c1, and  $N_{\text{catalog}}$  is gained by normalizing the number of the corresponding earthquakes in the 1997–2016 GCMT catalog to 100-year timescale, shown as blue circles in Figure 2c1. For the magnitude ranges with a high threshold magnitude (Mw7.1–7.9), the forecast results deviate a little from the situation shown by the actual seismic catalog (Figure 2c1): For the threshold magnitudes of Mw7.1–7.3, the success rates of the forecast results are about 70%; for the threshold magnitudes of Mw7.4–7.7, the success rates are close to 50%; for the threshold magnitudes of Mw7.8–7.9, the success rates lie between 30% and 40% (Figure 2c2). As the time span of the catalog used for the forecast is only 20 years, the number of Mw7.0+ earthquakes in the India-Eurasia collision zone in the catalog is relatively small, which somewhat affects the robustness of the forecast results for the threshold magnitudes of Mw7.1–7.9. While the amount of Mw6.0–7.0 earthquakes is relatively adequate, the forecast results for the threshold magnitudes of Mw6.0–7.0 should have good robustness. This part of the forecast results is generally consistent with the actual seismic catalog (Figure 2c1), and most success rates are over 80%, nearly half of which are over 90% (Figure 2c2), implying that the forecast results have a good reliability. Note that our final forecast results, such as those in Figure 1, are based on the whole 1977–2016 GCMT catalog. As time goes on, the GCMT catalog with longer time span should be used in the forecast to further improve the robustness of the forecast results.

### 3.2. Implication for Block Versus Continuum Models

Contrast views (block vs. continuum models) exist on how continent deforms in the India-Eurasia collision zone after decades of studies: Block model suggests that deformation is mainly localized on the major faults which separate crustal blocks (e.g., Avouac & Tapponnier, 1993; Loveless & Meade, 2011; Thatcher, 2007); continuum model argues that deformation is continuously distributed throughout the entire lithosphere (e.g., England & Houseman, 1986; England & Molnar, 2005; Flesch et al., 2001).

The forecast results can describe the seismicity level throughout time. Higher forecast values imply more frequent earthquakes; thus, the corresponding regions are more active and farther to the standard of rigid blocks. Here we suggest that shallow seismicity forecast can provide a promising approach to help us distinguish between block and continuum models for different areas.

Figures 1a–1d all show that the distribution of high forecast values is generally consistent with the scope of the Tibetan Plateau, Tien Shan, West Mongolia, North China, and Myanmar, implying that the tectonic environments of these regions are active; thus, we suggest that block motion cannot well describe their kinematics. In contrast, the forecast values in Tarim, Gobi-Alashan, Ordos, Junggar, Amur, and South China are relatively low, even for the  $M_w \geq 6.0$  earthquakes as shown in Figure 1d, and these regions have no major active faults identified within them, indicating that their tectonic environments are stable; thus, we argue that block model may be able to provide an approximate description of the crustal movement in these regions.

### 3.3. Implication for Seismic Gaps

The forecast results can reflect the seismicity which should occur in the past. If some regions with high forecast values are lack of historical earthquakes, it means that such regions are undergoing high earthquake risk and can be regarded as seismic gaps. In the following, we will describe two obvious examples—the west-central Himalaya and the central Altyn Tagh fault, shown as black ellipses in Figure 1a.

#### 3.3.1. The West-Central Himalaya

Some early studies identified the segment between the 1905 Mw7.9 Kangra and the 1934 Mw8.0 Nepal-Bihar ruptures of the Himalaya as a seismic gap (e.g., Khattri, 1987; Khattri & Tyagi, 1983). Recently, the 2015 Mw7.8 Gorkha earthquake occurred at the eastern edge of this gap (Avouac et al., 2015; Bilham, 2015). The west-central Himalaya we refer to is the stretch between the rupture zones of the 1905 and the 2015 earthquakes. It is a major region where the highest forecast values lie (Figures 1a–1d). However, since the 1505 Mw8.2 Mustang earthquake (Ambraseys & Jackson, 2003; Jackson, 2002), only two  $M_w \geq 7.5$  earthquakes, the 1720 Mw7.5 Delhi and the 1803 Mw7.5 Kumaon earthquakes, occurred in the west-central Himalaya according to the historical seismic catalog as shown in Figure 1a. This frequency is even lower than that of the Xianshuihe-Xiaojiang fault system, where the forecast values are significantly lower

(Figures 1a–1d) and  $M_w \geq 7.5$  earthquakes are in fact overdue (Shan et al., 2013; Wen et al., 2008). Thus, it is no doubt that the west-central Himalaya is overdue for  $M_w \geq 7.5$  earthquakes, possibly  $M_w \geq 8.0$  due to that the geomorphic features of foothills and river terraces along the Himalaya imply that multiple great earthquakes at  $M_w \geq 8.0$  occurred in the past (Bilham et al., 2001). Some studies argued that  $M_w \geq 9.0$  great earthquakes may occur in the Himalaya (e.g., Bilham & Wallace, 2005; Stevens & Avouac, 2016). Stevens and Avouac (2016) indicated that the average cycle of such great earthquakes is about 800 years. In any case, the fact is that most accumulated strain energy since the 1505 earthquake has not been released, which is now able to generate an earthquake approximately equal to the 1505 earthquake (Ambraseys & Jackson, 2003; Bilham & Ambraseys, 2004).

### 3.3.2. The Central Altyn Tagh Fault

The Altyn Tagh fault is somewhat comparable to the San Andreas fault, bounding the strong Tarim Basin to the north, comparable to the Pacific plate, and the weak Tibetan Plateau to the south, comparable to the North American continent (Molnar & Tapponnier, 1975; Yin & Harrison, 2000). As shown in Figures 1a–1d, the forecast values along the central Altyn Tagh fault are high, but only two  $M_w \geq 7.0$  earthquakes, the 1924  $M_w 7.0$  Minfeng and the 1924  $M_w 7.2$  Minfeng earthquakes, are recorded near its western edge, and there are no  $M_w \geq 7.5$  earthquakes according to the historical seismic catalog. Considering that the Xianshuihe-Xiaojiang fault system with comparable forecast values has more frequent  $M_w \geq 7.0$  and  $M_w \geq 7.5$  earthquakes (Figures 1a and 1b) but is actually overdue for such earthquakes (Shan et al., 2013; Wen et al., 2008), we suggest that the central Altyn Tagh fault can be regarded as a gap of large earthquakes at  $M_w \geq 7.0$  and  $M_w \geq 7.5$ . Some studies also mentioned that the central Altyn Tagh fault calls for special attention (e.g., Xu et al., 2017). Note that relatively complete seismic catalog began in the 20th century, we may miss some earlier earthquakes in the historical seismic catalog; thus, further field investigations will be necessary.

## 4. Conclusions

We apply the method in Bird and Kreemer (2015) to forecast the shallow seismicity of the India-Eurasia collision zone with the latest geodetic strain rate field presented in Zheng et al. (2017) and the 1977–2016 GCMT catalog, and infer that the region would suffer from about 11  $M_w \geq 7.5$ , 36  $M_w \geq 7.0$ , 109  $M_w \geq 6.5$ , and 326  $M_w \geq 6.0$  shallow earthquakes every 100 years. Our forecast results based on the 1977–2016 GCMT catalog have a good consistency with the actual situation shown by this catalog.

We compare the forecast results only based on the 1977–1996 GCMT catalog with the actual situation shown by the 1997–2016 GCMT catalog, and find that the forecast results for the magnitude ranges with threshold magnitudes of  $M_w 7.1$ – $7.9$  deviate a little from the actual catalog, which may be due to that the time span of 20 years is too short to include enough  $M_w 7.0+$  earthquakes, while the forecast results for  $M_w 6.0$ – $7.0$  threshold magnitudes are close to the actual catalog.

We suggest that shallow seismicity forecast may provide a promising approach to help distinguish between block and continuum models, and block model may be able to describe the crustal movement in Tarim, Gobi-Alashan, Ordos, Junggar, Amur, and South China approximately.

We indicate that the regions with high-forecasted earthquake rates but lack of historical earthquakes can be regarded as seismic gaps, such as the west-central Himalaya that is overdue for  $M_w \geq 7.5$  earthquakes, possibly  $M_w \geq 8.0$ , and the central Altyn Tagh fault that is overdue for  $M_w \geq 7.0$  and  $M_w \geq 7.5$  earthquakes.

### Acknowledgments

The GPS data set supporting this paper is available in Zheng et al. (2017). We appreciate the very helpful guidance and advice from Peter Bird and David D. Jackson at University of California, Los Angeles. Also, we are greatly grateful to Peter Bird for his constructive reviews which help improve this manuscript. This work was supported by National Key R&D Program of China (2017YFC1500501), National Science Foundation of China (41672205, 41774036, and 41674033) and Natural Science Foundation of Hubei Province of China (2018CFA052).

## References

- Ambraseys, N., & Jackson, D. (2003). A note on early earthquakes in northern India and southern Tibet. *Current Science*, 84(4), 570–582.
- Ambraseys, N. N., & Douglas, J. (2004). Magnitude calibration of north Indian earthquakes. *Geophysical Journal International*, 159(1), 165–206. <https://doi.org/10.1111/j.1365-246X.2004.02323.x>
- Avouac, J.-P., Meng, L., Wei, S., Wang, T., & Ampuero, J.-P. (2015). Lower edge of locked Main Himalayan Thrust unzipped by the 2015 Gorkha earthquake. *Nature Geoscience*, 8(9), 708–711. <https://doi.org/10.1038/ngeo2518>
- Avouac, J.-P., & Tapponnier, P. (1993). Kinematic model of active deformation in Central Asia. *Geophysical Research Letters*, 20(10), 895–898. <https://doi.org/10.1029/93GL00128>
- Bilham, R. (2010). Lessons from the Haiti earthquake. *Nature*, 463(7283), 878–879. <https://doi.org/10.1038/463878a>
- Bilham, R. (2015). Seismology: Raising Kathmandu. *Nature Geoscience*, 8(8), 582–584. <https://doi.org/10.1038/ngeo2498>

- Bilham, R., & Ambraseys, N. (2004). Apparent Himalayan slip deficit from the summation of seismic moments for Himalayan earthquakes, 1500–2000. *Current Science*, 88(10), 1658–1663.
- Bilham, R., Gaur, V. K., & Molnar, P. (2001). Himalayan seismic hazard. *Science*, 293(5534), 1442–1444. <https://doi.org/10.1126/science.1062584>
- Bilham, R., & Wallace, K. (2005). Future Mw > 8 earthquakes in the Himalaya: Implications from the 26 Dec 2004 Mw = 9.0 earthquake on India's eastern plate margin. *Geological Survey of India Special Publication*, 85, 1–14.
- Bird, P. (2003). An updated digital model of plate boundaries. *Geochemistry, Geophysics, Geosystems*, 4(3), 1027. <https://doi.org/10.1029/2001GC000252>
- Bird, P., Jackson, D. D., Kagan, Y. Y., Kreemer, C., & Stein, R. S. (2015). GEAR1: A global earthquake activity rate model constructed from geodetic strain rates and smoothed seismicity. *Bulletin of the Seismological Society of America*, 105(5), 2538–2554. <https://doi.org/10.1785/0120150058>
- Bird, P., & Kagan, Y. Y. (2004). Plate-tectonic analysis of shallow seismicity: Apparent boundary width, beta, corner magnitude, coupled lithosphere thickness, and coupling in seven tectonic settings. *Bulletin of the Seismological Society of America*, 94(6), 2380–2399. <https://doi.org/10.1785/0120030107>
- Bird, P., & Kreemer, C. (2015). Revised tectonic forecast of global shallow seismicity based on version 2.1 of the Global Strain Rate Map. *Bulletin of the Seismological Society of America*, 105(1), 152–166. <https://doi.org/10.1785/0120140129>
- Bird, P., Kreemer, C., & Holt, W. E. (2010). A long-term forecast of shallow seismicity based on the Global Strain Rate Map. *Seismological Research Letters*, 81(2), 184–194. <https://doi.org/10.1785/gssrl.81.2.184>
- Bird, P., & Liu, Z. (2007). Seismic hazard inferred from tectonics: California. *Seismological Research Letters*, 78(1), 37–48. <https://doi.org/10.1785/gssrl.78.1.37>
- Calais, E., Camelbeeck, T., Stein, S., Liu, M., & Craig, T. J. (2016). A new paradigm for large earthquakes in stable continental plate interiors. *Geophysical Research Letters*, 43, 10,621–10,637. <https://doi.org/10.1002/2016GL070815>
- Division of Earthquake Monitoring and Prediction (DEMP) (1995). *Catalogue of Chinese historical strong earthquakes (in Chinese)*. Beijing: Seismological Press.
- England, P., & Houseman, G. (1986). Finite strain calculations of continental deformation. 2. Comparison with the India-Asia collision zone. *Journal of Geophysical Research*, 91(B3), 3664–3676. <https://doi.org/10.1029/JB091iB03p03664>
- England, P., & Jackson, J. (2011). Uncharted seismic risk. *Nature Geoscience*, 4(6), 348–349. <https://doi.org/10.1038/ngeo1168>
- England, P., & Molnar, P. (2005). Late Quaternary to decadal velocity fields in Asia. *Journal of Geophysical Research*, 110, B12401. <https://doi.org/10.1029/2004JB003541>
- Field, E. H., Biasi, G. P., Bird, P., Dawson, T. E., Felzer, K. R., Jackson, D. D., et al. (2013). Uniform California earthquake rupture forecast, version 3 (UCERF3): The time-independent model. U.S. Geological Survey Open-File Report 2013-1165 (California Geological Survey Special Report 228, and Southern California Earthquake Center Publication 1792), 97 pp. <https://doi.org/10.3133/ofr20131165>
- Flesch, L. M., John Haines, A., & Holt, W. E. (2001). Dynamics of the India-Eurasia collision zone. *Journal of Geophysical Research: Solid Earth*, 106(B8), 16,435–16,460. <https://doi.org/10.1029/2001JB000208>
- Jackson, D. (2002). The great western-Himalayan earthquake of 1505: A rupture of the central Himalayan gap? In H. Blezer (Ed.), *Tibet, past and present* (pp. 147–159). Leiden: Brill's Tibetan Studies Library.
- Johnston, A. C. (1996). Seismic moment assessment of earthquakes in stable continental regions—II. Historical seismicity. *Geophysical Journal International*, 125(3), 639–678. <https://doi.org/10.1111/j.1365-246X.1996.tb06015.x>
- Johnston, A. C., Kanter, L. R., Coppersmith, K. J., & Cornell, C. A. (1994). *The earthquakes of stable continental regions (Technical Report 102261)*. Palo Alto, CA: Electric Power Research Institute.
- Kagan, Y. Y., Bird, P., & Jackson, D. D. (2010). Earthquake patterns in diverse tectonic zones of the globe. *Pure and Applied Geophysics*, 167(6–7), 721–741. <https://doi.org/10.1007/s00024-010-0075-3>
- Kagan, Y. Y., & Jackson, D. D. (1994). Long-term probabilistic forecasting of earthquakes. *Journal of Geophysical Research*, 99(B7), 13,685–13,700. <https://doi.org/10.1029/94JB00500>
- Kagan, Y. Y., & Jackson, D. D. (2000). Probabilistic forecasting of earthquakes. *Geophysical Journal International*, 143(2), 438–453. <https://doi.org/10.1046/j.1365-246X.2000.01267.x>
- Kagan, Y. Y., & Jackson, D. D. (2011). Global earthquake forecasts. *Geophysical Journal International*, 184(2), 759–776. <https://doi.org/10.1111/j.1365-246X.2010.04857.x>
- Khattari, K. N. (1987). Great earthquakes, seismicity gaps and potential for earthquake disaster along the Himalaya plate boundary. *Tectonophysics*, 138(1), 79–92. [https://doi.org/10.1016/0040-1951\(87\)90067-9](https://doi.org/10.1016/0040-1951(87)90067-9)
- Khattari, K. N., & Tyagi, A. K. (1983). Seismicity patterns in the Himalayan plate boundary and identification of areas of high seismic potential. *Tectonophysics*, 96(3–4), 281–297. [https://doi.org/10.1016/0040-1951\(83\)90222-6](https://doi.org/10.1016/0040-1951(83)90222-6)
- Kreemer, C., Blewitt, G., & Klein, E. C. (2014). A geodetic plate motion and Global Strain Rate Model. *Geochemistry, Geophysics, Geosystems*, 15, 3849–3889. <https://doi.org/10.1002/2014GC005407>
- Kreemer, C., Holt, W. E., & John Haines, A. (2003). An integrated global model of present-day plate motions and plate boundary deformation. *Geophysical Journal International*, 154(1), 8–34. <https://doi.org/10.1046/j.1365-246X.2003.01917.x>
- Loveless, J. P., & Meade, B. J. (2011). Partitioning of localized and diffuse deformation in the Tibetan Plateau from joint inversions of geologic and geodetic observations. *Earth and Planetary Science Letters*, 303(1–2), 11–24. <https://doi.org/10.1016/j.epsl.2010.12.014>
- Molnar, P., & Tapponnier, P. (1975). Cenozoic tectonics of Asia: Effects of a continental collision. *Science*, 189(4201), 419–426. <https://doi.org/10.1126/science.189.4201.419>
- Petersen, M. D., Zeng, Y., Haller, K. M., McCaffrey, R., Hammond, W. C., Bird, P., et al. (2014). Geodesy- and geology-based slip-rate models for the western United States (excluding California) national seismic hazard maps. U.S Geological Survey Open-File Report 2013-1293, 80 pp. <https://doi.org/10.3133/ofr20131293>
- Shan, B., Xiong, X., Wang, R., Zheng, Y., & Yang, S. (2013). Coulomb stress evolution along Xianshuihe-Xiaojiang Fault System since 1713 and its interaction with Wenchuan earthquake, May 12, 2008. *Earth and Planetary Science Letters*, 377–378(5), 199–210. <https://doi.org/10.1016/j.epsl.2013.06.044>
- Stevens, V. L., & Avouac, J.-P. (2016). Millenary Mw > 9.0 earthquakes required by geodetic strain in the Himalaya. *Geophysical Research Letters*, 43, 1118–1123. <https://doi.org/10.1002/2015GL067336>
- Tapponnier, P., & Molnar, P. (1977). Active faulting and tectonics in China. *Journal of Geophysical Research*, 82(20), 2905–2930. <https://doi.org/10.1029/JB082i020p02905>
- Thatcher, W. (2007). Microplate model for the present-day deformation of Tibet. *Journal of Geophysical Research*, 112, B01401. <https://doi.org/10.1029/2005JB004244>

- Wang, Q., Jackson, D. D., & Kagan, Y. Y. (2011). California earthquake forecasts based on smoothed seismicity: Model choices. *Bulletin of the Seismological Society of America*, 101(3), 1422–1430. <https://doi.org/10.1785/0120100125>
- Wen, X. Z., Ma, S.-L., Xu, X.-W., & He, Y.-N. (2008). Historical pattern and behavior of earthquake ruptures along the eastern boundary of the Sichuan-Yunan faulted-block, southwestern China. *Physics of the Earth and Planetary Interiors*, 168(1–2), 16–36. <https://doi.org/10.1016/j.pepi.2008.04.013>
- Xu, X.-W., Wu, X.-Y., Yu, G.-H., Tan, X.-B., & Li, K. (2017). Seismo-geological signatures for identifying  $M \geq 7.0$  earthquake risk areas and their preliminary application in mainland China (in Chinese). *Seismology and Geology*, 39(2), 219–275. <https://doi.org/10.3969/j.issn.0253-4967.2017.02.001>
- Yin, A., & Harrison, T. M. (2000). Geological evolution of the Himalayan-Tibetan orogeny. *Annual Review of Earth and Planetary Sciences*, 28(1), 211–280. <https://doi.org/10.1146/annurev.earth.28.1.211>
- Zheng, G., Wang, H., Wright, T. J., Lou, Y., Zhang, R., Zhang, W., et al. (2017). Crustal deformation in the India-Eurasia collision zone from 25 years of GPS measurements. *Journal of Geophysical Research: Solid Earth*, 122, 9290–9312. <https://doi.org/10.1002/2017JB014465>